

7 Studies of light scattering by complex particles using the null-field method with discrete sources

Thomas Wriedt

7.1 Introduction

Light scattering has an increasing importance in modern technologies. Examples are characterization of particles in natural or technical environments, surface characterization, biomedical sensing and nanotechnology. As a consequence, the development of accurate and fast methods devoted to the numerical simulation of electromagnetic and light scattering has become of fundamental importance.

There is a long interest in light scattering computations for nonspherical natural or artificial particles. To perform scattering computations the T-matrix method is considered of advantage because in the T-matrix all information on the polarization scattering effects is included. Thus from a precomputed T-matrix a scattering problem under slightly different conditions of incident wave orientation or scattering angles can quite easily be computed. There are also efficient ways to compute orientation-averaged scattering quantities from a precomputed T-matrix.

Although there has been much development in the T-matrix method over the last two decades there still have been problems with scattering computations for some types of particles. These include arbitrarily shaped nonaxisymmetric particles, particles having a large aspect ratio such as finite fibres or flat discs, and compound particles consisting of regions of different refractive indices. Other problems have been with chiral or optically anisotropic particles.

In the recent development of the Null-Field Method with Discrete Sources (NFM-DS) all of the method problems mentioned have been solved. In the standard T-matrix method a single system of spherical vector wave functions is used for internal field expansions. In the NFM-DS different kinds of discrete sources having different positions can be used for field expansion and this helps to overcome the stability problems with the standard method.

In this chapter the development of the Null-Field Method with Discrete Sources will be reviewed and some exemplary scattering results will be presented to demonstrate the capabilities of the concept. Recent developments will be mentioned.

First we give a short review of the state of the art of the Discrete Sources Method as well as the T-Matrix Method. Next we will introduce the Null-Field method with Discrete Sources as an extension of these two methods.

7.2 Discrete Sources Method

The Discrete Sources Method (DSM) [1] and related methods are widely used techniques for the numerical solution of elliptic boundary value problems including electromagnetic scattering.

The main idea of the DSM consists of approximating the solution of the problem by a linear combination of discrete sources. These discrete sources are the fundamental solution of the differential equation of the problem. The introduction of the Discrete Sources Method is generally attributed to Kupradze and Aleksidze [2].

Since that time the method has been applied in various fields such as acoustics, elasticity theory, electromagnetism, fluid dynamics, geophysics and solid mechanics. For a full theoretical outline of the method we refer the interested reader to the book by Doicu, Eremin and Wriedt [3]. An excellent review of the DSM and related methods for elliptic boundary value problems over recent decades has been given by Fairweather and Karageorghis [4]. Fairweather, Karageorghis and Martin [5] also surveyed the DSM applications in scattering and radiation problems. An edited volume covering different variants of this method has been published by Wriedt [6].

The DSM method is able to solve the problem of scattering from arbitrary shaped scatterers. Using point matching or point collocation of the boundary condition on the surface of the scatterer the original problem is reduced to determining the unknown coefficients of the discrete sources by solving a linear system of equations. The coefficients can also be obtained by matching the fields at the boundaries of the regions using a least squares fit of the boundary data. In this way the scattered field can be expressed in terms of a complete set of discrete sources.

There are various other names used for similar kind of concepts such as Charge Simulation Method [7], Yasuura Method [8], Multiple Multipole Program [9], Method of Auxiliary Sources [10], Discrete Singularity Method [11], Fictitious Sources Method [12], Method of Fictitious Sources [13], Method of Fundamental Solutions [14], and Generalized Multipole Technique [15].

The advantage of the Discrete Sources Method is that it provides a reduction in the size of the linear system that has to be solved and thus leads to a reduction in the computation time and memory storage.

The representation of electromagnetic fields by the use of discrete sources placed apart from the surface of the scatterer helps to simulate scattering by complex particles which cannot be solved using the standard T-matrix method. These particles include elongated scatterers, flat scatterers and concave scatterers. Compared to the surface integral method it does not have the problems encountered with singularities of the kernels. The method includes the possibility

of checking the accuracy of the computational results by means of a boundary matching error. The method also allows free choice of the kind and the location of the discrete sources, but if optimization of the coordinates of the discrete sources is included in the computational algorithms this would lead to a time consuming nonlinear least-squares minimization procedure. Another advantage of the DSM over other methods is that it does not require an elaborate discretization of the surface of the scatterer as in the Boundary Element Method (BEM); also integrations over the particle boundary surface, as needed in the T-matrix method, are avoided.

7.3 T-matrix method

The T-matrix method is a widely used method for obtaining numerical solutions to electromagnetic scattering problems. The T-matrix method found a wide range of applications because a corresponding FORTRAN program for a conducting scatterer had already been published in the early 1970s [16] which was later extended by others to the dielectric case. The T-matrix method is also called the Null-Field Method (NFM) or Extended Boundary Condition Method (EBCM). It is based on a series of papers by Waterman [17]. An early collection of conference papers on this method was edited by Varadan and Varadan [18]. With this method the incident, transmitted and scattered field is expanded into a series of spherical vector wavefunctions as shown for the scattered field:

$$\mathbf{E}_s(\mathbf{x}) = \sum_{\nu=1}^{\infty} f_{\nu} \mathbf{M}_{\nu}^3(k_s \mathbf{x}) + g_{\nu} \mathbf{N}_{\nu}^3(k_s \mathbf{x}), \quad (7.1)$$

$$\begin{bmatrix} f_{\nu} \\ g_{\nu} \end{bmatrix} = \mathbf{T} \begin{bmatrix} a_{\nu}^0 \\ b_{\nu}^0 \end{bmatrix}. \quad (7.2)$$

In this equation \mathbf{N}_{ν}^3 and \mathbf{M}_{ν}^3 represent the radiating spherical vector wavefunctions. The expansion coefficients of the scattered field f_{ν} , g_{ν} are related to the coefficients of the incident field a_{ν}^0 , b_{ν}^0 by the T-matrix (transition matrix).

The elements of the T-matrix are obtained by numerical integration. For an arbitrarily shaped particle lacking rotational symmetry a surface integral has to be computed. As this is computationally expensive, most implementations of the method are restricted to axisymmetric scatterers. In this case line integrals have to be computed. Nevertheless, there are some papers in which the T-matrix method has been applied to arbitrarily shaped scatterers. Early scattering computation for nonaxisymmetric scatterers using the T-matrix method have been done by P. W. Barber in his Ph.D. thesis [19] and by Schneider and Peden [20], both presenting results for ellipsoids. Wriedt and Doicu [21] presented computational examples with results of scattering by a dielectric cube of size parameter 2. A 3D variant of the T-matrix method has also been developed by Laitinen and Lumme [22] and by Kahnert et al. [23] both presenting scattering results for rounded cubes and another implementation was published by Havemann and Baran [24] giving results for hexagonal ice crystals.

A review of the status of the T-matrix approach up to 1996 has been published by Mishchenko, Travis and Mackowski [25]. A more recent review can be found in the book by Mishchenko, Hovenier and Travis [26]. The T-matrix method is also subject of books by Mishchenko et al. [27] and Borghese et al. [28]. A database of the literature on the T-matrix method has recently been compiled by Mishchenko et al. [29].

The notion of a T-matrix of a single scatterer makes it possible to solve problems of scattering from an arbitrary number of homogeneous objects also in the vicinity of a plane surface through the use of the T-matrix formalism. This method fully takes into account the interaction between the objects from multiple scattering and can deal with a large number of scattering particles. This feature, computing the T-matrix for a group of scatterers from the T-matrix of each constituent, makes the method very powerful and is considered its main advantages over other methods.

It has been found that the numerical performance of the T-matrix method is strongly dependent on the shape of the scatterer. It tends to degrade as the shape deviates from a sphere. An efficient approach for overcoming the numerical-instability problem in computing the T-matrix for highly nonspherical particles is the Null-Field Method with Discrete Sources, which is introduced in the next section.

7.4 Null-Field method with Discrete Sources

The Null-Field Method with Discrete Sources (NFM-DS) was originally developed to solve the stability problems in the standard T-matrix method with elongated and flat particles.

In this section we would like to outline the basics of the Null-field Method with Discrete Sources [3]. Let us consider a three-dimensional space D consisting of the union of a closed surface S , its interior D_i and its exterior D_s . We denote by k_t the wave number in the domain D_t , where $k_t = k\sqrt{\varepsilon_t\mu_t}$, $k = \omega/c$, $t = s, i$ and ε_t is the permeability, μ_t is the permittivity.

The transmission boundary-value problem can be formulated as follows. Let $\mathbf{E}_0, \mathbf{H}_0$ be an entire solution to the Maxwell equations representing an incident electromagnetic field. Find the vector fields, $\mathbf{E}_s, \mathbf{H}_s \in C^1(D_s) \cap C(\overline{D}_s)$ and $\mathbf{E}_i, \mathbf{H}_i \in C^1(D_i) \cap C(\overline{D}_i)$ satisfying the Maxwell's equations

$$\begin{aligned}\nabla \times \mathbf{E}_t &= jk\mu_t\mathbf{H}_t, \\ \nabla \times \mathbf{H}_t &= -jk\varepsilon_t\mathbf{E}_t,\end{aligned}\tag{7.3}$$

in D_t , where $t = s, i$; $j = \sqrt{-1}$ and two boundary conditions:

$$\begin{aligned}\mathbf{n} \times \mathbf{E}_i - \mathbf{n} \times \mathbf{E}_s &= \mathbf{n} \times \mathbf{E}_0, \\ \mathbf{n} \times \mathbf{H}_i - \mathbf{n} \times \mathbf{H}_s &= \mathbf{n} \times \mathbf{H}_0,\end{aligned}\tag{7.4}$$

on S , where \mathbf{n} is the outward directing normal to the boundary. In addition, the scattered fields $\mathbf{E}_s, \mathbf{H}_s$ must satisfy the Silver-Müller radiation condition uniformly for all directions \mathbf{x}/x .

For solving the transmission boundary-value problem in the framework of the NFM-DS the scattering object is replaced by a set of surface current densities \mathbf{e} and \mathbf{h} , so that in the exterior domain the sources and fields are exactly the same as those existing in the original scattering problem. The entire analysis can conveniently be broken down into the following three steps:

(I) A set of integral equations for the surface current densities \mathbf{e} and \mathbf{h} is derived for a variety of discrete sources. Physically, the set of integral equations in question guarantees the null-field condition within D_i . It is noted that localized and distributed vector spherical functions, magnetic and electric dipoles or vector Mie-potentials can be used as discrete sources. Essentially, the NFM-DS consists in the projection relations:

$$\begin{aligned} \int_S \left[(\mathbf{e} - \mathbf{e}_0) \cdot \boldsymbol{\Psi}_\nu^3 + j \sqrt{\frac{\mu_s}{\varepsilon_s}} (\mathbf{h} - \mathbf{h}_0) \cdot \boldsymbol{\Phi}_\nu^3 \right] dS &= 0 \\ \int_S \left[(\mathbf{e} - \mathbf{e}_0) \cdot \boldsymbol{\Phi}_\nu^3 + j \sqrt{\frac{\mu_s}{\varepsilon_s}} (\mathbf{h} - \mathbf{h}_0) \cdot \boldsymbol{\Psi}_\nu^3 \right] dS &= 0, \quad \nu = 1, 2, \dots \end{aligned} \quad (7.5)$$

where $\mathbf{e}_0 = \mathbf{n} \times \mathbf{E}_0$ and $\mathbf{h}_0 = \mathbf{n} \times \mathbf{H}_0$ are the tangential components of the incident electric and magnetic fields. The set $\{\boldsymbol{\Psi}_\nu^3, \boldsymbol{\Phi}_\nu^3\}_{\nu=1,2,\dots}$ consists of radiating solutions to Maxwell equations and depends on the system of discrete sources which is used for imposing the null-field condition. Actually, this set together with the set of regular solutions to Maxwell equations $\{\boldsymbol{\Psi}_\nu^1, \boldsymbol{\Phi}_\nu^1\}_{\nu=1,2,\dots}$ stands for

– localized vector spherical functions $\{\mathbf{M}_{mn}^{1,3}, \mathbf{N}_{mn}^{1,3}\}_{m \in \mathbb{Z}, n \geq \max(1, |m|)}$,

$$\begin{aligned} \mathbf{M}_{mn}^{1,3}(k\mathbf{x}) &= \sqrt{D_{mn} z_n(kr)} \left[jm \frac{P_n^{|m|}(\cos \theta)}{\sin \theta} \mathbf{e}_\theta - \frac{dP_n^{|m|}(\cos \theta)}{d\theta} \mathbf{e}_\varphi \right] e^{jm\varphi}, \\ \mathbf{N}_{mn}^{1,3}(k\mathbf{x}) &= \sqrt{D_{mn}} \left\{ n(n+1) \frac{z_n(kr)}{kr} P_n^{|m|}(\cos \theta) e^{jm\varphi} \mathbf{e}_r \right. \\ &\quad \left. + \frac{[kr z_n(kr)]'}{kr} \left[\frac{dP_n^{|m|}(\cos \theta)}{d\theta} \mathbf{e}_\theta + jm \frac{P_n^{|m|}(\cos \theta)}{\sin \theta} \mathbf{e}_\varphi \right] \right\} e^{jm\varphi}, \end{aligned} \quad (7.6)$$

where $(\mathbf{e}_r, \mathbf{e}_\theta, \mathbf{e}_\varphi)$ are the unit vectors in spherical coordinates (r, θ, φ) , z_n designates the spherical Bessel functions j_n or the spherical Hankel functions of the first kind h_n^1 , $P_n^{|m|}$ denotes the associated Legendre polynomial of order n and m , and D_{mn} is a normalization constant given by

$$D_{mn} = \frac{2n+1}{4n(n+1)} \cdot \frac{(n-|m|)!}{(n+|m|)!}, \quad (7.7)$$

– distributed vector spherical functions $\{\mathcal{M}_{mn}^{1,3}, \mathcal{N}_{mn}^{1,3}\}_{m \in \mathbb{Z}, n=1,2,\dots}$:

$$\begin{aligned} \mathcal{M}_{mn}^{1,3}(k\mathbf{x}) &= \mathbf{M}_{m,|m|+l}^{1,3}(k(\mathbf{x}-z_n\mathbf{e}_3)), \quad \mathbf{x} \in \mathbb{R}^3 - \{z_n\mathbf{e}_3\}_{n=1}^\infty, \\ \mathcal{N}_{mn}^{1,3}(k\mathbf{x}) &= \mathbf{N}_{m,|m|+l}^{1,3}(k(\mathbf{x}-z_n\mathbf{e}_3)), \quad \mathbf{x} \in \mathbb{R}^3 - \{z_n\mathbf{e}_3\}_{n=1}^\infty, \end{aligned} \quad (7.8)$$

where $m \in \mathbb{Z}^0$, $n = 1, 2, \dots$; $l = 1$ if $m = 0$ and $l = 0$ if $m \neq 0$, and $\{z_n\}_{n=1}^\infty$ is a set of points located on a segment Γ_z of the z -axis,

– magnetic and electric dipoles $\left\{ \mathcal{M}_{ni}^{1,3}, \mathcal{N}_{ni}^{1,3} \right\}_{n=1,2,\dots,i=1,2} :$

$$\begin{aligned} \mathcal{M}_{ni}^{1,3}(k\mathbf{x}) &= \mathbf{m}(\mathbf{x}_n^\pm, \mathbf{x}, \tau_{ni}^\pm), \mathbf{x} \in \mathbb{R}^3 - \{\mathbf{x}_n^\pm\}_{n=1}^\infty, \\ \mathcal{N}_{ni}^{1,3}(k\mathbf{x}) &= \mathbf{n}(\mathbf{x}_n^\pm, \mathbf{x}, \tau_{ni}^\pm), \mathbf{x} \in \mathbb{R}^3 - \{\mathbf{x}_n^\pm\}_{n=1}^\infty, \end{aligned} \quad (7.9)$$

where $n = 1, 2, \dots$; $i = 1, 2, \dots$; τ_{n1} and τ_{n2} are two tangential linear independent unit vectors at the point \mathbf{x}_n ,

$$\mathbf{m}(\mathbf{x}, \mathbf{y}, \mathbf{a}) = \frac{1}{k^2} \mathbf{a}(\mathbf{x}) \times \nabla_{\mathbf{y}} g(\mathbf{x}, \mathbf{y}, k), \quad \mathbf{n}(\mathbf{x}, \mathbf{y}, \mathbf{a}) = \frac{1}{k} \nabla_{\mathbf{y}} \times \mathbf{m}(\mathbf{x}, \mathbf{y}, \mathbf{a}), \quad \mathbf{x} \neq \mathbf{y}, \quad (7.10)$$

and the sequence $\{\mathbf{x}_n^-\}_{n=1}^\infty$ is dense on a smooth surface S^- enclosed in D_i , while the sequence $\{\mathbf{x}_n^+\}_{n=1}^\infty$ is dense on a smooth surface S^+ enclosing D_i , or finally for the set of

– vector Mie-potentials $\left\{ \mathcal{M}_n^{1,3}, \mathcal{N}_n^{1,3} \right\}_{n=1,2,\dots} :$

$$\begin{aligned} \mathcal{M}_n^{1,3}(k\mathbf{x}) &= \frac{1}{k} \nabla \varphi_n^\pm(\mathbf{x}) \times \mathbf{x}, \quad \mathbf{x} \in \mathbb{R}^3 - \{\mathbf{x}_n^\pm\}_{n=1}^\infty, \\ \mathcal{N}_n^{1,3}(k\mathbf{x}) &= \frac{1}{k} \nabla \times \mathcal{M}_n^{1,3}(k\mathbf{x}), \quad \mathbf{x} \in \mathbb{R}^3 - \{\mathbf{x}_n^\pm\}_{n=1}^\infty, \end{aligned} \quad (7.11)$$

where the Green functions

$$\varphi_n^\pm(\mathbf{x}) = g(\mathbf{x}_n^\pm, \mathbf{x}, k), \quad n = 1, 2, \dots$$

have singularities $\{\mathbf{x}_n^-\}_{n=1}^\infty$ and $\{\mathbf{x}_n^+\}_{n=1}^\infty$ distributed on the auxiliary surfaces S^- and S^+ , respectively. By convention, when we refer to the null-field equations (7.5) we implicitly refer to all equivalent forms of these equations.

(II) The surface current densities are approximated by fields of discrete sources. In this context let \mathbf{e} and \mathbf{h} solve the null-field equations (7.5) and assume that the system $\{\mathbf{n} \times \mathbf{\Psi}_\mu^1, \mathbf{n} \times \mathbf{\Phi}_\mu^1\}_{\mu=1}^\infty$ forms a Schauder basis in $\mathcal{L}_{\tan}^2(S)$. Then there exists a sequence $\{a_\mu, b_\mu\}_{\mu=1}^\infty$ such that

$$\begin{aligned} \mathbf{e}(\mathbf{y}) &= \sum_{\mu=1}^\infty a_\mu \mathbf{n} \times \mathbf{\Psi}_\mu^1(k_i \mathbf{y}) + b_\mu \mathbf{n} \times \mathbf{\Phi}_\mu^1(k_i \mathbf{y}), \quad \mathbf{y} \in S, \\ \mathbf{h}(\mathbf{y}) &= -j \sqrt{\frac{\varepsilon_i}{\mu_i}} \sum_{\mu=1}^\infty a_\mu \mathbf{n} \times \mathbf{\Phi}_\mu^1(k_i \mathbf{y}) + b_\mu \mathbf{n} \times \mathbf{\Psi}_\mu^1(k_i \mathbf{y}), \quad \mathbf{y} \in S. \end{aligned} \quad (7.12)$$

We recall that a system $\{\psi_i\}_{i=1}^\infty$ is called a Schauder basis of a Banach space X if any element $u \in X$ can be uniquely represented as $u = \sum_{i=1}^\infty \alpha_i \psi_i$, where the convergence of the series is in the norm of X . It is noted that in the case of localized vector spherical functions the notion of Schauder basis is closely connected with the Rayleigh hypothesis. This hypothesis says that the series representation of the scattered field in terms of radiating localized vector spherical functions, which uniformly converges outside the circumscribing sphere, also converges on S .

(III) Once the surface current densities are determined the scattered field outside the circumscribing sphere is obtained by using the Stratton–Chu representation theorem. We get the series representation

$$\mathbf{E}_s(\mathbf{x}) = \sum_{\nu=1}^{\infty} f_{\nu} \mathbf{M}_{\nu}^3(k_s \mathbf{x}) + g_{\nu} \mathbf{N}_{\nu}^3(k_s \mathbf{x}), \tag{7.13}$$

where

$$\begin{aligned} f_{\nu} &= \frac{jk_s^2}{\pi} \int_S \left[\mathbf{e}(\mathbf{y}) \cdot \mathbf{N}_{\bar{\nu}}^1(k_s \mathbf{y}) + j \sqrt{\frac{\mu_s}{\varepsilon_s}} \mathbf{h}(\mathbf{y}) \cdot \mathbf{M}_{\bar{\nu}}^1(k_s \mathbf{y}) \right] dS(\mathbf{y}), \\ g_{\nu} &= \frac{jk_s^2}{\pi} \int_S \left[\mathbf{e}(\mathbf{y}) \cdot \mathbf{M}_{\bar{\nu}}^1(k_s \mathbf{y}) + j \sqrt{\frac{\mu_s}{\varepsilon_s}} \mathbf{h}(\mathbf{y}) \cdot \mathbf{N}_{\bar{\nu}}^1(k_s \mathbf{y}) \right] dS(\mathbf{y}). \end{aligned} \tag{7.14}$$

Here, $\bar{\nu}$ is a complex index incorporating $-m$ and n , i.e. $\bar{\nu} = (-m, n)$.

7.4.1 T-matrix computation

Now, for deriving the T-matrix, let us assume that the incident field can be expressed inside a finite region containing S as a series of regular vector spherical functions

$$\begin{aligned} \mathbf{E}_0(\mathbf{x}) &= \sum_{\nu=1}^{\infty} a_{\nu}^0 \mathbf{M}_{\nu}^1(k_s \mathbf{x}) + b_{\nu}^0 \mathbf{N}_{\nu}^1(k_s \mathbf{x}), \\ \mathbf{H}_0(\mathbf{x}) &= -j \sqrt{\frac{\varepsilon_s}{\mu_s}} \sum_{\nu=1}^{\infty} a_{\nu}^0 \mathbf{N}_{\nu}^1(k_s \mathbf{x}) + b_{\nu}^0 \mathbf{M}_{\nu}^1(k_s \mathbf{x}). \end{aligned} \tag{7.15}$$

Then, using (7.5)–(7.15) we see that the relation between the scattered and the incident field coefficients is linear and is given by a transition matrix \mathbf{T} as follows

$$\begin{bmatrix} f_{\nu} \\ g_{\nu} \end{bmatrix} = \mathbf{T} \begin{bmatrix} a_{\nu}^0 \\ b_{\nu}^0 \end{bmatrix}. \tag{7.16}$$

Here

$$\mathbf{T} = \mathbf{B} \mathbf{A}^{-1} \mathbf{A}_0, \tag{7.17}$$

where \mathbf{A} , \mathbf{B} and \mathbf{A}_0 are block matrices written in general as

$$\mathbf{X} = \begin{bmatrix} X_{\nu\mu}^{11} & X_{\nu\mu}^{12} \\ X_{\nu\mu}^{21} & X_{\nu\mu}^{22} \end{bmatrix}, \nu, \mu = 1, 2, \dots, \tag{7.18}$$

with \mathbf{X} standing for \mathbf{A} , \mathbf{B} and \mathbf{A}_0 . Explicit expressions for the elements of these matrices are given by Doicu, Eremin and Wriedt [3].

It is noted that the exact, infinite T-matrix is independent of the expansion systems used on S . However, the approximate truncated matrix, computed according to

$$\mathbf{T}_N = \mathbf{B}_N \mathbf{A}_N^{-1} \mathbf{A}_{0N} \tag{7.19}$$

does contain such a dependence.

Energy characteristics in the far field are computed from the far-field pattern \mathbf{E}_{s0}^N for an unit amplitude incident electric field for p- or s-polarization. The angle-dependent intensity function plotted in the simulation section is the normalized differential scattering cross-section (DSCS)

$$\frac{\sigma_d}{\pi a^2} = \frac{|k_s \mathbf{E}_{s0}^N|^2}{\pi |k_s a|^2}, \quad (7.20)$$

where a is a characteristic dimension of the particle.

7.4.2 Orientation averaged scattering

To numerically compute orientation averaged scattering three integrals with respect to the three Euler angles α, β, γ have to be computed. Thus the value of interest $f(\alpha, \beta, \gamma)$ is integrated over all directions and polarization of the incident plane wave. The numerical procedure used to do this is based on a step wise procedure

$$\begin{aligned} & \int_0^{2\pi} \int_0^\pi \int_0^{2\pi} f(\alpha, \beta, \gamma) \sin \beta \, d\alpha \, d\beta \, d\gamma \\ & \approx 4\pi^3 \sum_{n_\alpha=1}^{N_\alpha} \sum_{n_\beta=1}^{N_\beta} \sum_{n_\gamma=1}^{N_\gamma} f(\alpha, \beta, \gamma) \sin(n_\beta \pi / N_\beta) \frac{n_\alpha n_\beta n_\gamma}{N_\alpha N_\beta N_\gamma}. \end{aligned} \quad (7.21)$$

The triple integral is converted to three summations. Angle α is digitized for N_α steps in the range $(0, 2\pi)$, angle β is digitized for N_β steps in the range $(0, \pi)$, and angle γ is digitized for N_γ steps in the range $(0, 2\pi)$.

7.4.3 Computation of surface integrals

In the NFM-DS method we use a polyhedral representation of the particle shape model of interest. This means that a particle shape is modeled by a closed surface formed by many planar triangles. Such shapes bounded by polygons are commonly used in computer graphics and there are different methods available to construct a polyhedral representation of implicit or parametric surfaces. In our case the representation by a triangular patch model should allow firstly a correct calculation of surface integrals and secondly a graphical visualization of the scattering particle.

Different methods are available to create a geometric surface mesh of a particle. For example the free *HyperFun* polygonizer software may be used for surface mesh generation [30]. It generates VRML output of a triangular patch model for implicit surfaces.

In the standard method to compute surface integrals a parametric equation is used and thus an equivalent integral in polar coordinates has to be evaluated. Thus partial derivatives of x, y, z with respect to the parametrization (in our case parameters ϑ, φ) are needed which may not be available analytically. If the

partial derivatives are not available, a numerical method via finite differences may be used.

We use an alternative approach based on a modified centroid quadrature that does not use the partial derivatives. This modified centroid quadrature has been proposed and investigated by Georg and Tauch [31]. The surface integrals to be computed are approximated by

$$\int_S f \, dS \approx \sum_i f(v_{i,c}) \, \text{area}[v_{i,1}, v_{i,2}, v_{i,3}]. \quad (7.22)$$

Here, $v_{i,1}, v_{i,2}, v_{i,3}$ are the vertices spanning a triangle and point $v_{i,c}$ denotes the centre of mass of the triangle $[v_{i,1}, v_{i,2}, v_{i,3}]$ given by

$$v_{i,c} = \frac{1}{3} \sum_{j=1}^3 v_{i,j}. \quad (7.23)$$

Thus the integral over each triangle is approximated by multiplying the value of the integrand at the centroid by the triangle area.

7.5 Scattering by complex particles

In this section we would like to present some exemplary scattering results for complex particles using the NFM-DS. We will show computational results and in some cases validation results obtained using other computational programs. More information on the method of validation of the developed programs will be given in the next section on validation.

7.5.1 Fibres

Field expansion using discrete sources helps very much when computing scattering by very elongated scatterers such as finite rotational symmetric fibres. With such type of scatterers the discrete sources are positioned on the axis of symmetry of the particle. As an example of an elongated particle we are considering a long circular cylinder which is rounded at the bottom and the top. The shape of this fibre is presented in Fig. 7.1.

In polar coordinates this fibre shape is described by the following equations:

$$\begin{aligned} r &= a \cos \theta \pm \sqrt{b^2 - a^2 \sin^2 \theta} \quad \text{for } 0 \leq \theta \leq \arctan\left(\frac{b}{a}\right) \\ r &= \frac{b}{\sin \theta} \quad \text{for } \arctan\left(\frac{b}{a}\right) < \theta < \arctan\left(\frac{-a}{b}\right) \\ r &= -a \cos \theta \pm \sqrt{b^2 - a^2 \sin^2 \theta} \quad \text{for } \arctan\left(\frac{-a}{b}\right) \leq \theta \leq \pi \end{aligned}$$

So the total length of the fibre is $2(a + b)$ and its diameter is $2b$.

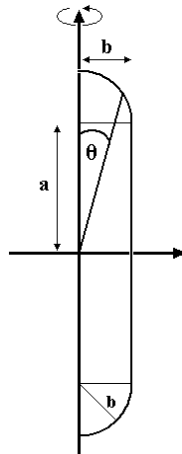


Fig. 7.1. Geometry of a fibre.

Light scattering computations of fibre-like particles are of interest for various scientific branches: astrophysics, atmospheric science, optical particle characterization – the latter especially in connection with airborne fibrous particles like mineral, glass or asbestos fibres, which are considered to cause serious health hazards. Here high aspect ratios are of special interest and so it is required that a light scattering simulation algorithm can handle them. Figure 7.2 presents the differential scattering cross-section (DSCS) of such a fibre and demonstrates

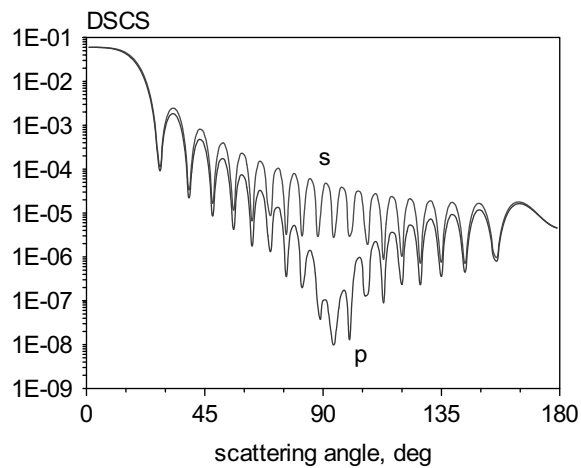


Fig. 7.2. Differential scattering cross-section of a fibre particle with length $2(a + b) = 6 \mu\text{m}$ and diameter $2b = 0.12 \mu\text{m}$. Incident wavelength is $\lambda = 632.8 \text{ nm}$, refractive index $n = 1.5$.

the capabilities of using discrete sources in the T-matrix method for fibre-like particles.

The total length of the fibre is $6\ \mu\text{m}$ and the diameter is $0.12\ \mu\text{m}$ which leads to an aspect ratio of 50:1, which is an already challenging value. The incident wavelength is 632.8nm and the refractive index is 1.5. The plane wave is incident onto the long side of the fibre. Convergent computational results were achieved using 50 discrete sources and 3,000 surface points to compute the line integrals.

Further computational results have been published by Pulbere and Wriedt [32].

7.5.2 Flat plates

Application of discrete sources also helps in computing scattering by oblate particles which are very flat. In this case the discrete sources have to be arranged in the complex plane [33]. As an exemplary particle we use a flat circular disc which is rounded at its edges. The geometry of such disc is shown in Fig. 7.3.

This particle shape can be described in polar coordinates by the following equations:

$$\begin{aligned} r &= \frac{a}{\cos \theta} \quad \text{for } 0 \leq \theta \leq \arctan\left(\frac{b}{a}\right), \\ r &= a \cos \theta \pm \sqrt{b^2 - a^2 \sin^2 \theta} \quad \text{for } \arctan\left(\frac{b}{a}\right) < \theta < \arctan\left(\frac{-a}{b}\right), \\ r &= -\frac{a}{\cos \theta} \quad \text{for } \arctan\left(\frac{-a}{b}\right) \leq \theta \leq \pi. \end{aligned}$$

For this shape we also would like to present scattering results. As an example we computed scattering by a flat circular disc having a total diameter of $6\ \mu\text{m}$ and a thickness of $0.06\ \mu\text{m}$. This results in an extremely high aspect ratio of 100 : 1. Figure 7.4 presents the corresponding scattering pattern. The incident wavelength is 632.8nm and refractive index is 1.5. The plane wave is incident onto the flat side of the disc. To achieve this convergent computational result 36 discrete sources were needed and the number of integration points needed is 5,000. Further scattering patterns of such flat particles have been published by Hellmers et al. [34].

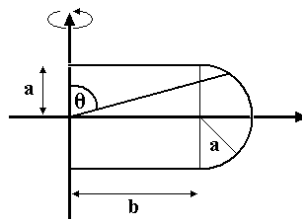


Fig. 7.3. Geometry of an oblate circular disc.

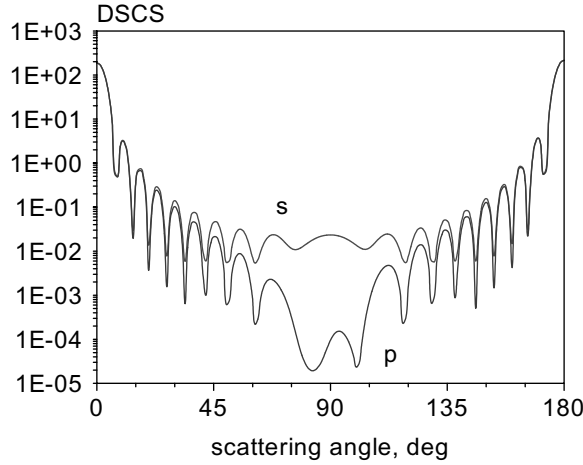


Fig. 7.4. Differential scattering cross-section of an oblate circular disc with a radius of $2(a+b) = 6 \mu\text{m}$ and a thickness of $2a = 0.06 \mu\text{m}$. Incident wavelength $\lambda = 632.8 \text{ nm}$, refractive index $n = 1.5$.

7.5.3 Cassini ovals

The particle shapes investigated so far have been convex in its shape. With NFM-DS it is also possible to calculate scattering by concave shapes, which has till now been considered hardly possible using a standard T-matrix algorithm. To demonstrate this we make use of Cassini ovals. This kind of curves was introduced by Giovanni Domenico Cassini (1625–1712), also known as Jean-Dominique Cassini, in 1680. These curves are characterized in such a way that the product of the distance of two fixed focal points is constant (while for a normal ellipse the sum of the distance of two fixed focal points is constant).

The Cassini ovals have the Cartesian equation:

$$\left[(x-a)^2 + y^2 \right] \left[(x+a)^2 + y^2 \right] = b^4.$$

This leads to:

$$y = \pm \left(-a^2 - x^2 \pm (4x^2a^2 + b^4)^{\frac{1}{2}} \right)^{\frac{1}{2}}. \quad (7.24)$$

The corresponding expression in polar coordinates is

$$r = \left(a^2 - 2a^2 \sin(\theta)^2 + (-4a^4 \sin(\theta)^2 + 4a^4 \sin(\theta)^4 + b^4)^{\frac{1}{2}} \right)^{\frac{1}{2}}.$$

The Cassini shape therefore depends on the relation b/a (Fig. 7.5).

If $a < b$ the curve is an oval loop, for $a = b$ the result is a lemniscate (like the ∞ -symbol) and for $a > b$ the curve consists of two separate loops. If a is chosen slightly smaller than b one gets a concave, bone-like shape. The concavity on both sides will get deeper the closer a gets to b . By rotating this two-dimensional

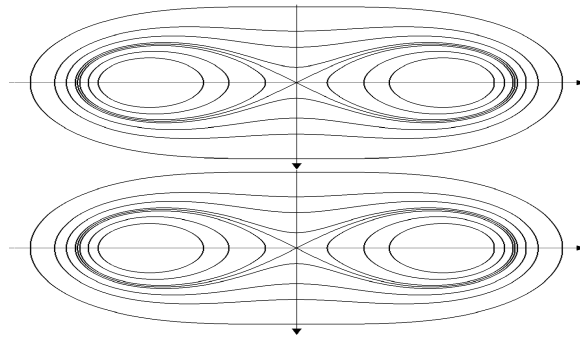


Fig. 7.5. Cassini ovals for a given a and varying values of b .

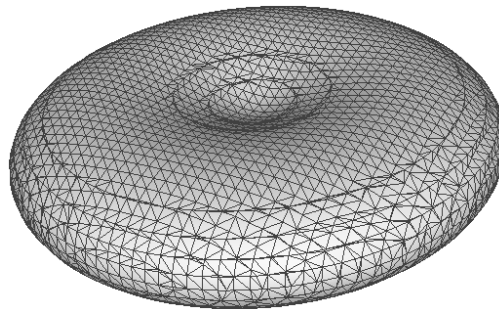


Fig. 7.6. 3D shape of a Cassini oval.

curve around the vertical axis we get a three-dimensional particle of the shape of an oblate disc with a concavity on its top and bottom (Fig. 7.6). To get more flexibility and to manipulate the thickness directly a factor c can be introduced as the first term in equation (7.24).

Figure 7.7 shows the light scattering diagram for a Cassini oval based particle with $a = 1.1$, $b = 1.125$ and $c = 0.66$, which gives a total diameter of $3.15 \mu\text{m}$ and an aspect ratio of approximately 4:1. The incident wavelength is 632.8 nm and refractive index is 1.5. The plane wave is incident onto the flat side of the Cassini oval. For the computation 28 discrete sources positioned in complex plane were used and 1,000 points were needed for integration. Further computational results for concave particles have been published by Hellmers et al. [35] and Wriedt et al. [36].

7.5.4 Anisotropic particles

Colour pigments are commonly anisotropic in their refractive index. To be able to investigate scattering by such type of colour pigments the NFM-DS has been extended to compute scattering by uniaxial anisotropic particles [37]. The next scattering diagram (Fig. 7.8) presents scattering by an anisotropic sphere of di-

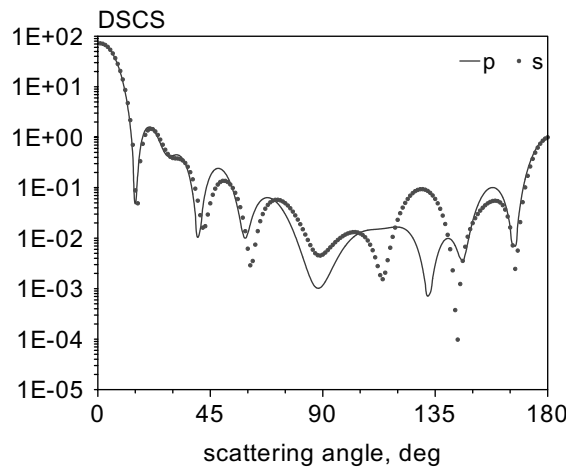


Fig. 7.7. Differential scattering cross-section of a Cassini oval with $a = 1.1$, $b = 1.125$ and $c = 0.66$. Incident wavelength is $\lambda = 632.8$ nm, refractive index is $n = 1.5$.

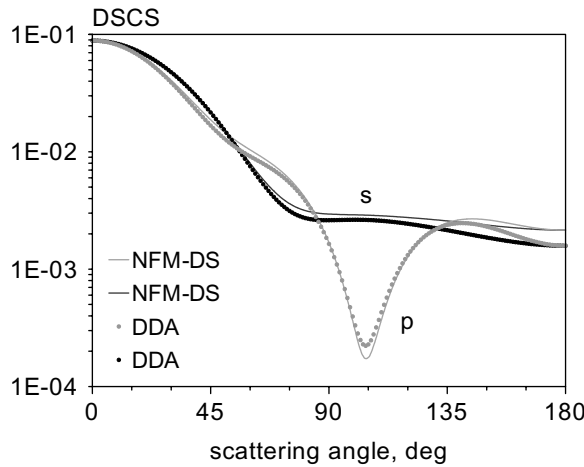


Fig. 7.8. Differential scattering cross section of an anisotropic sphere ($d = 400$ nm, $n_x = n_y = 2.5 + j0.725$, $n_z = 4.0 + j1.45$, $\lambda = 498$ nm).

iameter 400nm and refractive indices of $n_x = n_y = 2.5 + j0.725$, $n_z = 4.0 + j1.45$ alongside scattering results obtained from the DDSCAT program for validation. The plane electromagnetic wave is incident along the z -axis and the incident wavelength in this case is 498 nm. The figure demonstrates close agreement between the results of both programs. The related NFM-DS computer programs are also capable computing scattering by rotational symmetric uniaxial anisotropic particles as well as uniaxial anisotropic particles of arbitrary shape without rotational symmetry.

7.5.5 Arbitrarily shaped 3D particles

The NFM-DS sources can be used to compute light scattering by arbitrarily shaped 3D particles which lack rotational symmetry. Scattering results have been computed for cubes [21], ellipsoids [3], [38], superellipsoids [39], rough particles [39], and hexagonal prisms [40]. In each case the shape of the scattering particle has to be triangulated into a suitable surface patch model to compute the surface integrals. There are various tools in computational graphics available to handle this problem.

To perform a convergence check versus the number of integration points some flexibility in surface triangulation is needed. Thus methods to increase or reduce the number of surface patches are of great help. To increase the number of surface triangles, the divide by three and the divide by four schemes implemented in the a free DOS program Triangles by David Sharp [41] is suitable. To reduce the number of triangles the SIM Rational Reducer program by Systems in Motion AS [42] can be used.

As an example, scattering by a rounded hexagonal prism has been computed and the results have been compared to results obtained from MMP and CST Microwave Studio. The dimension of the rounded hexagonal prism are $l = 2\ \mu\text{m}$ (rectangular face to rectangular face), $d = 1.15471\ \mu\text{m}$ (hexagonal face to hexagonal face), the refractive index used is $n = 1.5$ and the wavelength of the incident plane wave is 628.319 nm. The plane wave is incident along the z -axis and the scattering results are plotted in the y, z scattering plane. The three-dimensional shape of the scattering hexagonal prism is plotted in Fig. 7.9. As can be seen from the scattering plots in Figs 7.10 and 7.11, there is almost perfect correspondence between the results of the different programs for p- as well as for s-polarization.

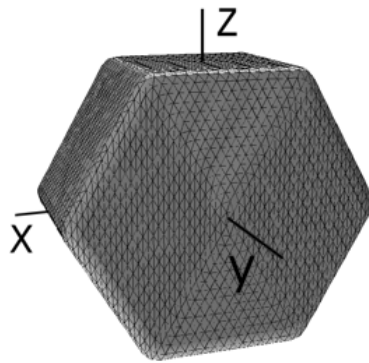


Fig. 7.9. Rounded hexagonal prism $l = 2\ \mu\text{m}$, $d = 1.15471\ \mu\text{m}$.

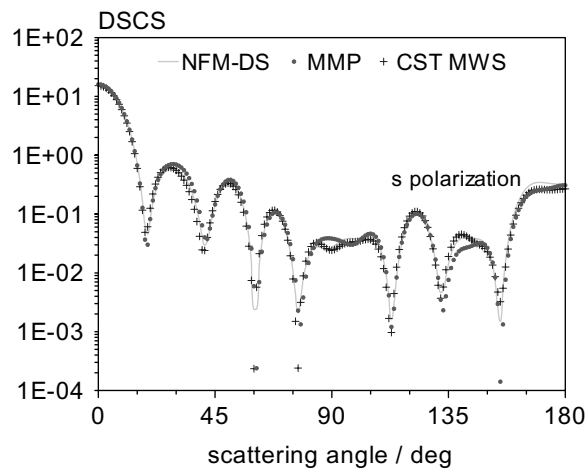


Fig. 7.10. Differential scattering cross-section of a rounded hexagonal prism $l = 2 \mu\text{m}$, $d = 1.15471 \mu\text{m}$, $n = 1.5$, $\lambda = 628.319 \text{ nm}$.

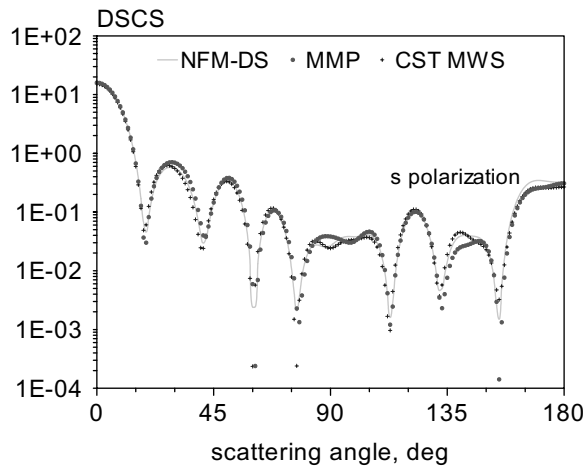


Fig. 7.11. Differential scattering cross-section of a rounded hexagonal prism $l = 2 \mu\text{m}$, $d = 1.15471 \mu\text{m}$, $n = 1.5$, $\lambda = 628.319 \text{ nm}$.

7.5.6 Agglomerates

Characterization of the size and the structure of agglomerates is also needed for many applications such as determination of soot in vehicle diesel exhaust or of aircraft exhaust soot in the atmosphere. For this angular distributions of light scattered by the particles are commonly measured and used for particle characterization. To compute scattering by such type of aggregates particle geometry data have to be generated using a cluster-cluster aggregation algorithm [43]. Figure 7.12 includes the geometry of an exemplary aggregate. The diameter of

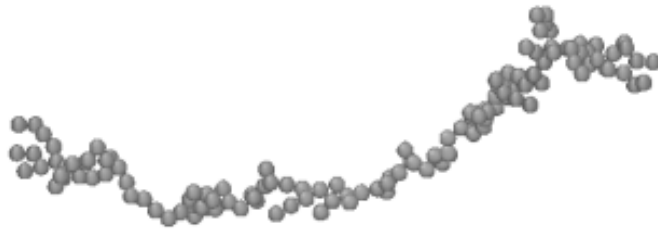


Fig. 7.12. Figure of cluster cluster aggregate with parameters diameter of primary particle $d = 30$ nm, fractal dimension $D_f = 1.3$, radius of gyration $r_g = 4.5462$ μm , 130 primary spheres.

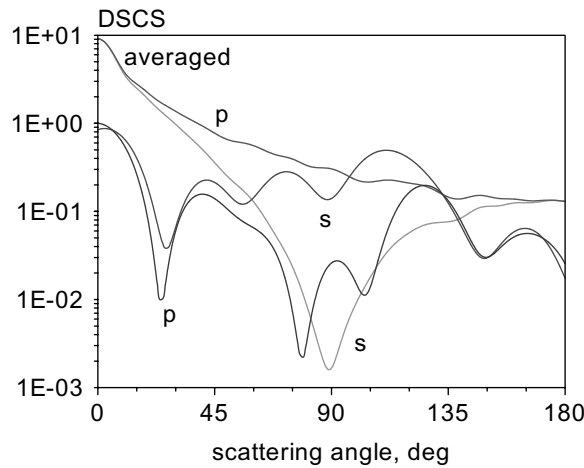


Fig. 7.13. Single scattering and orientation averaged DSCS of the cluster of Fig. 7.12 incident wavelength $\lambda = 514$ nm, soot refractive index $n = 1.57 + j0.56$.

primary particles is $d = 30$ nm, the fractal dimension is $D_f = 1.3$, and the radius of gyration is $r_g = 4.5462$ μm . There are in total 130 primary spheres in the aggregate. Figure 7.13 shows the differential scattering cross-section of this soot aggregate alongside orientation-averaged scattering. Orientation averaging leads to a damping of oscillations which are present in the single scattering diagram which resembles Rayleigh scattering.

7.5.7 Inclusions

Commonly with particles having inclusions, the T-matrix method is restricted to spherical inclusions. Using a multiple scattering approach we extended the NFM-DS to handle scattering by off-center nonspherical inclusions. A full description of the theory and additional computational results are available in Doicu and Wriedt [44] and Schuh and Wriedt [45].

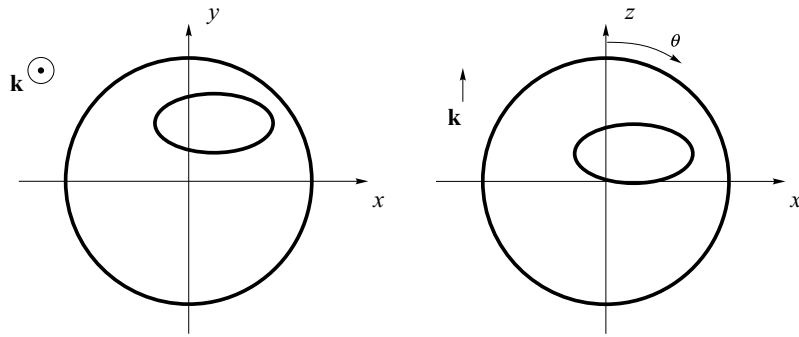


Fig. 7.14. Geometry of sphere with spheroidal inclusion, sphere size parameter $kr = 10$, spheroid size parameters $ka = 5$, $kb = 2.5$ placed at $kx_i = 2$, $ky_i = 4$, $kz_i = 2$; orientation Euler angles $\alpha = 0^\circ$, $\beta = 90^\circ$.

We consider a spherical particle with a spheroidal inclusion. The geometry of the scattering problem is shown in Fig. 7.14. The size parameter of the sphere is $kr = 10$, the refractive index is $n = 1.334$. The size parameters of the spheroid are $ka = 5$, $kb = 2.5$ placed at $kx_i = 2$, $ky_i = 4$, $kz_i = 2$; orientation Euler angles of the inclusion are $\alpha = 0^\circ$, $\beta = 90^\circ$. The refractive index of the inclusion is $n = 1.6$. In Figs 7.15 and 7.16, we plot the differential scattering cross-section computed with DFM-NS and the multiple multipole method for validation. There is close agreement between the two computational results.

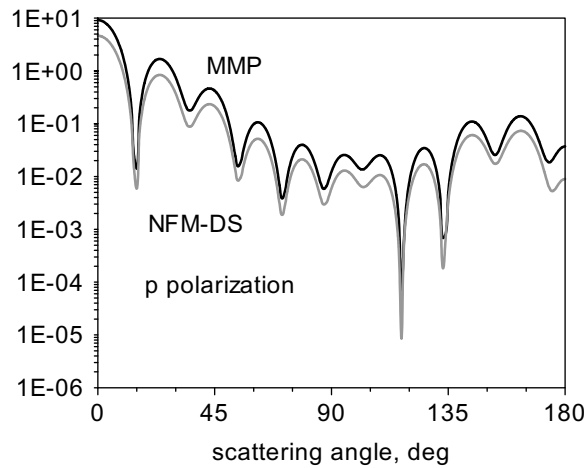


Fig. 7.15. DSCS of a sphere with a prolate spheroid inclusion with the scattering geometry of Fig. 7.14.

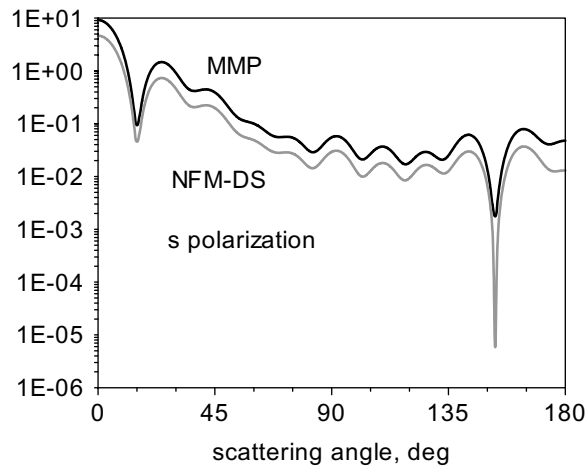


Fig. 7.16. DSCS of a sphere with a prolate spheroid inclusion with the scattering geometry of Fig. 7.14.

7.5.8 Particles on surfaces

Optical characterization of defects such as particles, bumps or pits on a silicon wafer surface is of great importance in semiconductor manufacturing. As semiconductor device dimensions become smaller, there is a need for optical wafer surface scanning systems to detect the size and composition of microcontaminations to sizes as low as $0.1\ \mu\text{m}$ or even smaller. To expand the current detection ability an efficient mathematical model and computer simulation technique is needed. There are some approximate approaches to computing scattering by a dielectric particle on a plane dielectric surface ([28] pp. 192).

But as these approaches are no longer sufficient for a modern design of particle surface scanners the NFM-DS has been extended to handle the particle surface scattering problem in an exact way. The theory is fully described in a book contribution by Doicu and Wriedt [46].

As an exemplary computational result, we present the scattering plot in Fig. 7.17 for a $1.09\ \mu\text{m}$ diameter polystyrene sphere on a plane silicon surface with the following parameters: sphere diameter $d = 1.09\ \mu\text{m}$, polystyrene refractive index $n = 1.64$, silicon refractive index $n = 4.90 + i3.84$, incident wavelength $\lambda = 308\ \text{nm}$. The plane wave is incident normal to the plane surface.

Plasmon resonance phenomena, that is the local amplification of light by nanoscale silver or gold noble particles, have potential applications for biosensors, bio-labels and nano-optical devices. Plasmon resonances of small noble metal spheres can be detected as peaks in the measured light scattering spectra. Transmission dark-field microscopy is a technique where only the particles scatter light into the direction of the microscope objective. Such a measuring device can visualize very small particles as coloured discs. The surface plasmon resonance frequency from a nonspherical particle or a particle aggregate

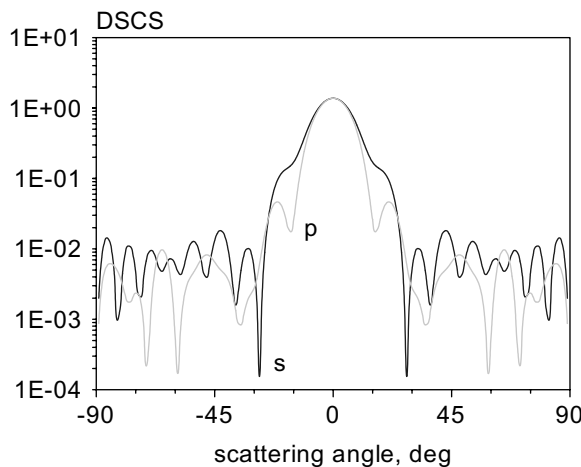


Fig. 7.17. DSCR of a sphere (diameter $d = 1.09 \mu\text{m}$, $n = 1.64$), on a plane silicon surface with $n = 4.90 + j3.84$ and an incident wavelength $\lambda = 308 \text{ nm}$.

is different compared to a single spherical particle. With this effect, measuring techniques which use white light illumination are capable of differentiating between aggregated particles and a single particle because of their different color. Even when bioreceptor molecules attached to a gold or silver sphere detect its biomolecular counterpart, the resonance frequency is shifted. In the following we give some simulation examples of particles on or near a plane surface. We compute intensities at different scattering angles over the visible spectrum of wavelengths of small particles with diameter $d = 80 \text{ nm}$. The intensities will be detector-integrated over a range of $\phi_{NA} = 25^\circ$ which corresponds to a numerical aperture of $NA = n \sin(\phi_{NA})$ of the objective lens. The particles consist of silver. The wavelength-dependent refractive indices are interpolated values from Johnson et al. [47]. The numerical aperture depends on the medium surrounding of the particle. The incident beam angle with respect to the normal is $\phi_0 = 30^\circ$ and the surrounding medium is water ($n = 1.333$).

From the computational results of the detector-integrated DSCS printed in Fig. 7.18 we see that the frequency and the form of the resonance peak very much depends on the distance of the silver particle from the plane silver surface. With a higher distance it shifts to a shorter wavelength and it also becomes broader.

7.6 Validation

An important step in development of the NFM-DS theory and the related computer programs is validation by comparing to results obtained from other programs. Although in scattering research measurement results were applied for validation of theory and corresponding programs [48] we did not consider this

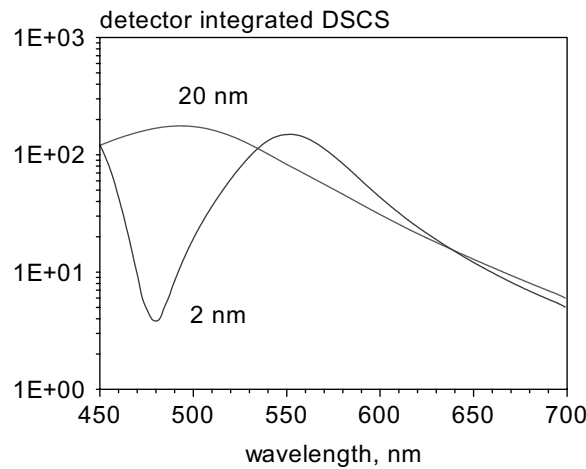


Fig. 7.18. Detector integrated DSCS of a silver sphere ($d = 80$ nm) on a silver plane surface with different heights of the particle.

as a suitable approach in our program development. In light scattering optics, it is much more difficult to obtain accurate measurements suitable for validation. Therefore we prefer to use other computation results for validation. Alongside validation it is, of course, important to care for convergence with respect to the number and order of discrete sources used in the simulation and with respect to the number of integration points used in computing the relevant surface integrals. The number of integration points proved to be much more stable than the number and order of discrete sources. In some cases we even found some plateau in the number and order of discrete sources where we obtained convergent scattering results. Increasing the number or order of discrete sources beyond this plateau again led to nonconvergence, which can make a convergence check somewhat tricky.

For program validation three different approaches have been used. In the first method, two different implementations of NFM-DS have been used for validation. For example, the program for the composite scatterers was compared to results of the multiple scattering program. In this case the composite particle consisted of three parts with the center part free space such that the problem could also be treated as a two-particle multiple scattering problem [40].

In the second approach we developed the Discrete Sources Method (DSM) together with the research group of Yuri Eremin, Lomonosov Moscow State University, for the same scattering problems. One may almost speak about co-evolution in program development. Examples are the flat disc [35], Cassini ovals [34], the long fibre [49] and total internal reflection microscopy (TIRM) [50].

In the third method we used other freely available programs for validation. In this we focused on three methods. These are Multiple Multipole Program (MMP) by Bomholt and Hafner [51], Discrete Dipole Approximation (DDA) [52] implemented in the FORTRAN program DDSCAT [53], and in various implementations of Finite Different Time Domain (FDTD) and the Volume Integral

Equation Method (VIEM) [54] and the related Finite Integration Technique FIT [55]. FIT is implemented in the commercial CST Microwave Studio program [56]. We also had a look at other commercial computational electromagnetics programs but found the CST Microwave Studio program to be the most suitable. With the other programs tested we hardly could input particle shape data or the program was restricted to small particle sizes compared to the incident wavelength. The reason for this is that with most programs not only the surface of a scatterer but the full volume of the scattering particle has to be discretized, which leads to a high demand in computer resources.

7.7 Applications

In this section we briefly mention the broad range of applications the computational programs based on NFM-DS have found in solving practical technological applications in recent years.

Phase Doppler Anemometry (PDA) was extended to size spheroidal particles [57,58]. The NFM-DS was used to develop an optical instrument for mineral and asbestos fibre characterization [32].

Extensive light scattering computations for aggregated particles helped to characterize soot particles in the flame of a Bunsen burner [43].

There is an ongoing project for characterization of red blood cells using light scattering [35]. Within a collaborative project total internal reflection microscopy (TIRM) for measurement of nanoforces acting on a colloidal particle near a plane surface has been developed [50]. Sensors for surface particle or surface defect characterization have been developed based on the NFM-DS.

7.8 Conclusion

In this chapter an overview of the progress in developing the NFM-DS has been given. Some open problems are still left. These include bi-anisotropic particles, bi-anisotropic host media, chiral media, nonaxisymmetric compound particles and optimal deposition of discrete sources and faces for surface integration.

Most of the FORTRAN programs developed within this project have been published on CD with a monograph on the Null-Field Method with Discrete Sources [40]. For further applications not covered by this review, such as chiral particles, layered particles [59], composite particles [60], Gaussian laser beam scattering [61], evanescent wave scattering [62] and dipole scattering the interested reader is referred to this book or to the cited papers.

Acknowledgments

I would like to thank Adrian Doicu for constant cooperation and Jens Hellmers, Roman Schuh, Norbert Riefler and Elena Eremina for providing computational results for this review. This work was supported by Deutsche Forschungsgemeinschaft (DFG).

7.9 Symbols and abbreviations

(a_ν^0, b_ν^0)	expansion coefficients of the incident field
(a_ν^0, b_ν^0)	expansion coefficients of the incident field
D_{mn}	normalization constant
$\mathbf{E}_0, \mathbf{E}_s$	incident and scattered fields
(\mathbf{e}, \mathbf{h})	surface current densities
(f_ν^0, g_ν^0)	expansion coefficients of the scattered field
k	wavenumber
$\{\mathbf{M}_{mn}^{1,3}, \mathbf{N}_{mn}^{1,3}\}$	localized vector spherical functions
$\{\mathcal{M}_{mn}^{1,3}, \mathcal{N}_{mn}^{1,3}\}$	distributed vector spherical functions
$\{\mathcal{M}_{ni}^{1,3}, \mathcal{N}_{ni}^{1,3}\}$	magnetic and electric dipoles
$\{\mathcal{M}_n^{1,3}, \mathcal{N}_n^{1,3}\}$	vector Mie-potentials
n	refractive index
S	particle surface
$[\mathbf{T}]$	transition matrix
(x, y, z)	Cartesian coordinate
\mathbf{x}	position vector
$\alpha_n^\pm(\mathbf{x})$	Green function
α, β, γ	Euler angles
(ϑ, φ)	angular coordinates
ϵ	permittivity
λ_0	wavelength in vacuum
$\sigma_d/\pi a^2$	normalized differential scattering cross-section (DSCS)
μ	permeability
v_i	vertex points on particle surface

References

1. Y. A. Eremin and A. G. Sveshnikov: A computer technology for the discrete source method in scattering problems. *Computational Mathematics and Modeling*, **14** (2003) 1, 16–25.
2. V. D. Kupradze and M. A. Aleksidze: The method of functional equations for the approximate solution of certain boundary value problems. *USSR Comput. Math. Math. Phys.*, **4** (1964) 4, 82–126.
3. A. Doicu, Y. A. Eremin, T. Wriedt: *Acoustic and Electromagnetic Scattering Analysis Using Discrete Sources*. Academic Press, San Diego 2000.
4. G. Fairweather and A. Karageorghis: The method of fundamental solutions for elliptic boundary value problems. *Adv. Comput. Math.*, **9** (1998), 69–95.
5. G. Fairweather, A. Karageorghis, P. A. Martin: The method of fundamental solutions for scattering and radiation problems. *Engineering Analysis with Boundary Elements*, **27** (2003), 759–769.
6. T. Wriedt (Ed.): *Generalized Multipole Techniques for Electromagnetic and Light Scattering*. Elsevier, Amsterdam 1999.
7. M. Katsurada, A mathematical study of the charge simulation method II, *J. Fac. Sci., Univ. of Tokyo, Sect. 1A, Math.* **36** (1989), 135–162.

8. M. Kawano, H. Ikuno, M. Nishimoto: Numerical analysis of 3-D scattering problems using the Yasuura method. *IEICE Trans. Electron.* **E79-C** (1996), 1358–1363.
9. Ch. Hafner, *Post-modern Electromagnetics Using Intelligent Maxwell Solvers*. John Wiley & Sons, Chichester 1999.
10. D. I. Kaklamani and H. T. Anastassiou: Aspects of the method of auxiliary sources in computational electromagnetics. *IEEE Antennas and Propagation Magazine* **44** (2002) 3, 48–64.
11. M. Nishimura, S. Takamatsu, and H. Shigesawa: A numerical analysis of electromagnetic scattering of perfect conducting cylinders by means of discrete singularity method improved by optimization process. *Electronics and Communications in Japan*, **67-B** (1984) 5, 552–558.
12. Y. Leviatan, Z. Baharav, E. Heyman: Analysis of electromagnetic scattering using arrays of fictitious sources. *IEEE Trans. Antennas Propagat.*, **AP-43** (1995) 10, 1091–1098.
13. D. Maystre, M. Saillard, G. Tayeb: Special methods of wave diffraction. in P. Sabatier and E.R. Pike (Eds): *Scattering*. Academic Press, London 2001.
14. M. A. Golberg and C. S. Chen: The method of fundamental solutions for potential, Helmholtz and diffusion problems. In M. A. Golberg (Ed.): *Boundary Integral Methods and Mathematical Aspects*. WIT Press/Computational Mechanics Publications, Boston 1999, 103–176.
15. A. C. Ludwig: The generalized multipole technique. *Comput. Phys. Commun.* **68** (1991), 306–314.
16. P. C. Waterman: Numerical solution of electromagnetic scattering problems. In R. Mittra: *Computer techniques for electromagnetics*. Pergamon Press, New York 1973, 97–157.
17. P. C. Waterman: Matrix formulation of electromagnetic scattering. *Proc. IEEE* **53** (1965), 803–812.
18. V. K. Varadan and V. V. Varadan (Ed): *Recent Developments in Classical Wave Scattering: Focus on the T-matrix*. Pergamon Press, Oxford 1980.
19. P. W. Barber: Differential scattering of electromagnetic waves by homogeneous isotropic dielectric bodies. Ph.D. thesis, University of California, Los Angeles 1973.
20. J. B. Schneider and I. C. Peden: Differential cross section of a dielectric ellipsoid by the T-matrix extended boundary condition method. *IEEE Trans. Antennas Propagat.* **AP 36** (1978), 1317–1321.
21. T. Wriedt and A. Doicu: Formulation of the extended boundary condition method for three-dimensional scattering using the method of discrete sources. *Journal of Modern Optics* **45** (1998) 1, 199–213.
22. H. Laitinen and K. Lumme: T-matrix method for general star-shaped particles: first results. *J. Quant. Spectrosc. Radiat. Transfer*, **60** (1998), 325–334.
23. F. M. Kahnert, J. J. Stammes, K. Stammes: Application of the extended boundary condition method to particles with sharp edges: a comparison of two surface integration approaches. *Applied Optics*, **40** (2001), 3101–3109.
24. S. Havemann and A. J. Baran: Extension of T-matrix to scattering of electromagnetic plane waves by non-axisymmetric dielectric particles: application to hexagonal ice cylinders. *J. Quant. Spectrosc. Radiat. Transfer*, **70** (2001), 139–158.
25. M. I. Mishchenko, L. D. Travis, D. W. Mackowski: T-matrix computations of light scattering by nonspherical particles: a review. *J Quant Spectrosc. Radiat. Transfer*, **55** (1996), 535–575.
26. M. I. Mishchenko, J. W. Hovenier, L. D. Travis (Eds): *Light Scattering by Nonspherical Particles*. Academic Press, San Diego 2000.

27. M. I. Mishchenko, L. D. Travis, A. A. Lacis: *Scattering, Absorption, and Emission of Light by Small Particles*. Cambridge University Press, Cambridge 2002.
28. F. Borghese, P. Dentl, R. Saija: *Scattering from Model Nonspherical Particles. Theory and Applications to Environmental Physics*. Springer Verlag, Berlin 2003.
29. M. I. Mishchenko, G. Videen, V. A. Babenko, N. G. Khlebtsov, T. Wriedt: T-matrix theory of electromagnetic scattering by particles and its applications: a comprehensive reference database. *J. Quant. Spectrosc. Radiat. Transfer*, **88** (2004), 357–406.
30. HyperFun Project, Language and Software Tools for F-rep Geometric Modeling. www.hyperfun.org.
31. K. Georg and J. Tausch: Some error estimates for the numerical approximation of surface integrals. *Math. Comp.*, **62** (1994), 755–763.
32. S. Pulbere, T. Wriedt: Light scattering by cylindrical fibers with high aspect ratio using the null-field method with discrete sources *Part. Part. Syst. Charact.*, **21** (2004), 213–218.
33. A. Doicu and T. Wriedt: Extended boundary condition method with multipole sources located in the complex plane. *Optics Commun.*, **139** (1997), 85–91.
34. J. Hellmers, T. Wriedt, A. Doicu: Light scattering simulation by oblate disc spheres using the null field method with discrete sources located in the complex plane. *Journal of Modern Optics*, **53** (2006) 3, 267–282.
35. J. Hellmers, E. Eremina, T. Wriedt: Simulation of light scattering by biconcave Cassini ovals using the nullfield method with discrete sources. *Journal of Optics A*, **8** (2006), 1–9.
36. T. Wriedt, J. Hellmers, E. Eremina, R. Schuh: Light scattering by single erythrocyte: Comparison of different methods. *J. Quant. Spectrosc. Radiat. Transfer*, **100** (2006), 444–456.
37. A. Doicu: Null-field method to electromagnetic scattering from uniaxial anisotropic particles. *Optics Commun.*, **218** (2003) 1–3, 11–17.
38. J. Hellmers and T. Wriedt: Influence of particle shape models on T-matrix light scattering simulation. *J. Quant. Spectrosc. Radiat. Transfer*, **89** (2004), 97–110.
39. T. Wriedt: Using the T-matrix method for light scattering computations by non-axisymmetric particles: Superellipsoids and realistically shaped particles. *Part. Part. Syst. Charact.*, **19** (2002) 4, 256–268.
40. A. Doicu, T. Wriedt, Yuri Eremin: *Light Scattering by Systems of Particles. Null-Field Method with Discrete Sources – Theory and Programs*. Springer Verlag, Berlin, Heidelberg, New York 2006.
41. Triangles, a triangle mesh construction utility: <http://www.geocities.com/Athens/Academy/8764/triangles.htm>.
42. Systems in Motion AS, www.sim.no.
43. N. Riefler, S. di Stasio, T. Wriedt: Structural analysis of clusters using configurational and orientational averaging in light scattering analysis. *J. Quant. Spectrosc. Radiat. Transfer*, **89** (2004), 323–342.
44. A. Doicu and T. Wriedt: T-matrix method for electromagnetic scattering from scatterers with complex structure. *J. Quant. Spectrosc. Radiat. Transfer*, **70** (2001), 663–673.
45. R. Schuh and T. Wriedt: Computer programs for light scattering by particles with inclusions. *J. Quant. Spectrosc. Radiat. Transfer*, **70** (2001), 715–723.
46. T. Wriedt and A. Doicu: T-matrix method for light scattering from particles on or near an infinite surface. in F. Moreno and F. González (Eds): *Light Scattering from Microstructures*. Springer Verlag, Berlin 2000, 113–132.

47. P. B. Johnson and R. W. Christy: Optical constants of noble metals. *Phys. Rev. B*, **6** (1972), 4370–4379.
48. A. Hizal and A. Marincic: New rigorous formulation of electromagnetic scattering from perfectly conducting bodies of arbitrary shape. *Proc. IEE*, **117** (1970) 8, 1639–1647.
49. E. Eremina, Y. Eremin, T. Wriedt: Review of light scattering by fiber particles with a high aspect ratio. *Recent Res. Devel. Optics*, **3** (2003), 297–318.
50. L. Helden, E. Eremina, N. Riefler, Ch. Hertlein, C. Bechinger, Y. Erimin, T. Wriedt: Single particle evanescent light scattering simulations for total internal reflection microscopy. *Applied Optics*, submitted.
51. Ch. Hafner and L. Bomholt: *The 3D Electromagnetic Wave Simulator, 3D MMP Software and User's Guide*. Wiley, Chichester 1993.
52. B. T. Draine and P. J. Flatau: Discrete-dipole approximation for scattering calculations. *J. Opt. Soc. Am. A*, **11** (1994), 1491–1499.
53. The Discrete Dipole Approximation for Scattering and Absorption of Light by Irregular Particles. www.astro.princeton.edu/~draine/DDSCAT.html.
54. T. Wriedt and U. Comberg: Comparison of computational scattering methods. *J. Quant. Spectrosc. Radiat. Transfer*, **60** (1998) 3, 411–423.
55. T. Weiland: A discretization method for the solution of Maxwell's equation for six-components fields. *Electron. Commun. AEÜ*, **31** (1977), 116–120.
56. Computer Simulation Technology GmbH, www.cst.de.
57. A. Doicu, T. Wriedt, K. Bauckhage: Light scattering by homogeneous axisymmetrical particles for PDA calculations to measure both axes of spheroidal particles. *Part. Part. Syst. Charact.*, **14** (1997), 3–11.
58. A. Doicu, J. Köser, T. Wriedt, K. Bauckhage: Light scattering simulation and measurement of monodisperse spheroids using a Phase Doppler Anemometer. *Part. Part. Syst. Charac.*, **15** (1999), 257–262.
59. A. Doicu and T. Wriedt: Null-field method with discrete sources to electromagnetic scattering from layered scatterers. *Comput. Phys. Commun.*, **138** (2001), 136–142.
60. A. Doicu and T. Wriedt: Null-field method with discrete sources to electromagnetic scattering from composite scatterers. *Optics Commun.*, **190** (2001), 13–17.
61. A. Doicu and T. Wriedt: Formulations of the extended boundary condition method for incident Gaussian beams using multiple multipole expansions. *Journal of Modern Optics*, **44** (1997) 4, 785–801.
62. A. Doicu, Yu. Eremin, T. Wriedt: Scattering of evanescent waves by a particle on or near a plane surface. *Comput. Phys. Commun.*, **134** (2001), 1–10.